Identifying the atomic configuration of the tip apex using STM and frequency-modulation AFM with CO on Pt(111)

O. Gretz⬤, A. J. Weymouth⬤,[*] and F. J. Giessibl⬤

Institute of Experimental and Applied Physics, Department of Physics, University of Regensburg, Regensburg 93053, Germany

We investigated the atomic structure of metal tips by scanning individual CO molecules adsorbed on Pt(111) using scanning tunneling microscopy (STM) and frequency-modulation atomic force microscopy (FM-AFM). When scanning very close over a CO molecule, the frontmost atoms of the tip can be individually resolved in both the FM-AFM image and in the STM image. This is in contrast to previous work where CO was adsorbed on a different substrate: Cu(111). In this previous study, individual atoms could not be observed in the raw STM image but only in FM-AFM. We discuss the mechanisms behind the higher spatial resolution in STM. On Cu(111), the occupied surface state plays a large role in STM images near the Fermi level, and as adsorbed CO repels the surface state, it appears as a wide trough in STM images. In contrast, Pt(111) lacks an occupied surface state and an adsorbed CO molecule appears as a peak. We investigate if CO bending strongly influences the STM images, concluding that the atomic resolution of the tip over Pt(111) is due to highly localized through-molecule tunneling and CO bending is insignificant for contrast formation. Modelling the current between the CO and front atoms of the tip supports our findings.

I. INTRODUCTION

Single carbon monoxide (CO) molecules have been used widely as tip terminations in high spatial resolution scanning tunneling microscopy (STM) [1] and particularly in atomic force microscopy (AFM) [2]. Picking up a single CO molecule at the end of a metal tip (forming a CO tip) has enabled submolecular resolution with frequency-modulation atomic force microscopy (FM-AFM). CO-tips have also been used in STM to achieve intramolecular resolution [3,4].

Conversely, when single CO molecules are adsorbed on a metal surface, they can be used to identify the number, configuration, and, with limitations, the chemical species of front atoms at the tip apex [5–8]. This technique is called carbon monoxide front atom identification (COFI) [5–7]. Understanding the apex of the probe tip is essential to interpreting high resolution images and comparing observations to simulation in STM, inelastic electron tunneling spectroscopy [9] and FM-AFM [10].

In the first publication about COFI by Welker *et al.* in 2012, a single CO molecule on Cu(111) imaged a metal tip [5] and the attractive features separated by several Angstroms in the FM-AFM image were initially interpreted as a reflection of the crystal orientation of a single atom at the tip apex [5]. In a follow-up article using COFI, Hofmann *et al.* analyzed

force-distance curves and showed that a Cu front atom at the apex could be clearly discriminated from a W or Fe front atom [8]. In 2014, Gao *et al.* and Schwarz *et al.* investigated CO adsorbed on NiO(100), asserting that multiple features separated by several Angstroms indicated a tip that terminated in multiple atoms, where each feature represented an atom at the apex [11,12]. In 2015, Emmrich *et al.* imaged both small iron clusters on Cu(111) with a CO tip and the inverse system, concluding that the multiple attractive features in the FM-AFM channel indicate tip apexes ending with multiple atoms [7] and correcting the initial interpretation of a correspondence of multiple extrema to the crystallographic orientation of the tip's front atom in Ref. [5]. Our current understanding is that when an adsorbed CO molecule is imaged with FM-AFM, the small and sharp CO molecule (the O atom has only 40% of the diameter of a typical metal atom) probes the number and configuration of atoms at the apex of a metal tip. The dangling bonds of the adatoms of Si(111)-(7 × 7) have also shown to create similar images of multiatom metal tips as CO/Cu(111) [6].

If COFI is performed on CO adsorbed to Cu(111), single Cu or Fe atom tips appear in FM-AFM images as attractive features with a repulsive ring around them, while, e.g., Si tip atoms would appear as single repulsions [13]. Individual atoms at the tip apex can be directly observed in the raw FM-AFM image but not in the raw STM images [5,8].

STM of CO on Cu(111) vs Pt(111)

Figures [1(a)] and [1(b)] compare STM images of a CO adsorbed on Cu(111) and Pt(111). On Cu, we observe a wide trough in the conductance over the adsorbate, whereas on Pt a narrow peak in the conductance appears over the adsorbed
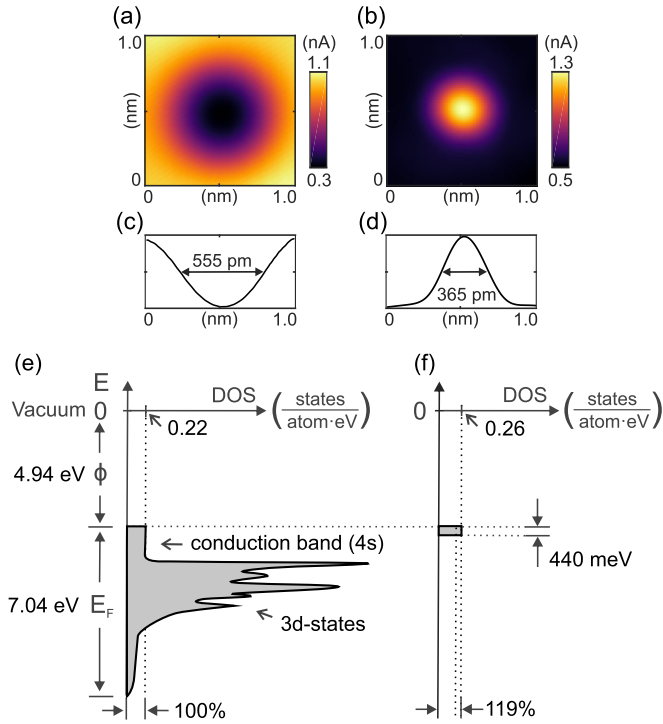
---

[*]jay.weymouth@ur.de

FIG. 1. Constant-height STM images of CO on Cu(111) with bias 10 mV (a) and Pt(111) (b) with bias 1 mV. Corresponding line profiles of (a) and (b) are plotted in (c) and (d), indicating the evaluated full width at half maximum as an estimate of the feature width. (e) Schematic plot of the density of states (DOS) for Cu bulk (see, e.g., Fig. 6 in Ref. [17]) and for the surface states (f) of Cu(111) (2D). The bulk DOS of Cu relates nicely to the electronic states of the free Cu atom. The valence shell configuration of Cu is given by $3d^{10}4s^1$, and the large DOS from about 1.3 eV to about 4.6 eV below the Fermi level are due to the ten $3d$ electrons per atom that constitute the $3d$ bands, while the conduction band that ends at the Fermi level originates from atomic $4s$ states. The $3d$ states are included in this sketch for completeness, although they are fully occupied and do not affect the density of states at the Fermi level. The surface state provides 0.26 states per surface atom and eV, while the $4s$-conduction band bulk states only provide 0.22 states per atom and eV.

CO. For the data shown in Figs. 1(a) and 1(b), the full width at half maximum of the trough on Cu(111) is 555 pm, shown in Fig. 1(c), and the peak on Pt(111) is 365 pm, shown in Fig. 1(d). We suggest that the stark difference of the STM contrast of CO on Cu(111) versus Pt(111) is due to the presence of a surface state with a high density of states on Cu(111) [14]. A simple estimate shows that the density of states of the surface state at the Fermi energy reaches 119% of the bulk value for Cu(111), while Pt(111) has an empty surface state [15].

In STM, the tunneling matrix element contains the density of states of the tip and the density of states of the sample. If the sample has an occupied surface state at the Fermi energy as in Cu(111), we need to consider the density of states at the Fermi level E_F of the bulk states and the surface states. Figure 1(e) shows a sketch of the density of states for Cu of the bulk (3D) and of the surface states (2D) [Fig. 1(f)]. Generally, the density of states of a three-dimensional electron gas as a

function of energy $D_{3D}(E)$ and of a two-dimensional electron gas $D_{2D}(E)$ can be written as follows [16]:

$$D_{3D}(E) = \frac{(2m_{3D}^*)^{3/2}}{2\pi^2\hbar^3}\sqrt{E} \quad (1)$$

$$D_{2D}(E) = \frac{m_{2D}^*}{\pi\hbar^2 L_z}, \quad (2)$$

where m_{2D}^* denotes the effective mass of the electrons in the surface state and m_{3D}^* is the effective mass for the bulk electrons. L_z is the thickness of the surface state, yielding the same unit for both $D_{3D}(E)$ and $D_{2D}(E)$ of number of states per volume (m^3) and energy (J).

The thickness of the surface state can be estimated by its vertical decay length $\lambda = 1/\kappa$, via the work function ϕ: $L_z \approx \lambda = 1/\kappa = \hbar/\sqrt{2m_e\phi}$. $D_{2D}(E)$ can then be written:

$$D_{2D}(E) = \frac{m_{2D}\sqrt{2\phi m_e}}{\pi\hbar^3}. \quad (3)$$

If we calculate the ratio of the density of states at the Fermi level (which is significant for STM at low bias voltages), $D_{2D}(E_F)/D_{3D}(E_F)$, this yields:

$$\frac{D_{2D}(E_F)}{D_{3D}(E_F)} = \pi\frac{m_{2D}^*\sqrt{m_e}}{(m_{3D}^*)^{3/2}}\left(\frac{\phi}{E_F}\right)^{1/2}. \quad (4)$$

In the case of Cu(111) $m_{2D}^* = 0.46\,m_e$ [18], $m_{3D}^* = 1.01\,m_e$ [19], $\phi = 4.94$ eV [20], and $E_F = 7.04$ eV [16]. In absolute numbers, we find for the bulk density of states $D_{3D}(E_F) = 1.16 \times 10^{47}$ states/(m^3J) or 0.22 states per atom and eV. The absolute surface density of states is $D_{2D}(E_F) = 1.38 \times 10^{47}$ states/(m^3J) or 0.26 states per atom and eV. Surprisingly, the density of states at the Fermi level for Cu is larger for the surface state than for the bulk states with a ratio of $D_{2D}/D_{3D} = 1.19$. Therefore, the surface states provide a larger contribution to the STM images of bare Cu(111) at low bias than the bulk states, giving rise to the typical standing wave images [21]. On Cu(111) an adsorbed CO molecule apparently repels the surface state, leading to the wide trough in the STM image [22]. For some tips, the CO molecule in the center of the trough even shows up as a small local peak (see Fig. 1E in Ref. [23]). The through-molecule current on Cu(111) can sometimes be made visible by Laplace filtering the current data (see Figs. 2A, C, and E in Ref. [5]). On Pt(111), the through molecule tunneling dominates and the conductance is higher over a CO molecule than over the bare Pt(111) surface [24].

Here, we use simultaneous STM and FM-AFM to image isolated CO molecules adsorbed on the Pt(111) surface with metal tips. For certain tips we observe several attractive features in the FM-AFM images, which we associate to multiple atoms at the apex, as on Cu(111) [7].

Surprisingly, we also observed corresponding high-conductance features in the STM images which we assign to the individual atoms of the apex. These high-conductance STM features can be reproduced by approximating the tunneling current by s waves at the position of each tip atom. This finding opens the possibility of characterizing tips at the atomic scale with STM using CO molecules adsorbed on Pt(111).

II. EXPERIMENTAL SETUP

Measurements were performed with a combined low temperature UHV FM-AFM and STM (CreaTec Fischer GmbH, Berlin, Germany) operating at 5.6 K in ultrahigh vacuum equipped with a qPlus sensor [25] (spring constant $k = 3627$ N/m, frequency $f_0 = 35\,813.6$ Hz, and quality factor $Q = 29\,439$). All experiments were performed with an amplitude of $A = 50$ pm. The sensor was equipped with a tungsten tip which was repeatedly poked into the Pt(111) surface to generate different tip apex configurations.

The Pt(111) surface was cleaned by several sputtering (Ar ions at 1.2 keV) and annealing (1300 K) cycles. The final anneal cycle was performed at 1070 K to reduce the diffusion of natural contaminations like carbon from the bulk to the surface. CO was leaked in at a partial pressure of 5×10^{-8} mbar for 5 min.

After a tip apex of interest was identified, three-dimensional frequency shift Δf and current I datasets were collected by acquiring sets of constant-height images. First, an isolated CO adsorbate was identified. Then we approached the molecule in 10 pm steps until the CO laterally moved. We retracted 10 pm and acquired the closest scan.

After each image, the tip-sample distance was increased by 10 pm until no Δf contrast was detected. From the three-dimensional Δf datasets, the normal force F_z was evaluated using the method introduced by Sader and Jarvis [26].

III. EXPERIMENTAL RESULTS AND DISCUSSION

Figures 2(a)–2(f) show I and F_z images at $z = 340$ pm, 220 pm, and 150 pm for a single-atom tip. Figure 2(s) is a sketch of a single-atom tip and a CO. The zero point $z = 0$ pm is defined by the tunneling conductance at point contact of $(12906\,\Omega)^{-1}$ at the lower turnaround point of the tip [27].

In Fig. 2(a), at $z = 340$ pm, the CO molecule appears as a single circular attractive feature. Closer to the surface at $z = 220$ pm, the attractive feature increases in intensity: The force minimum decreases to -150 pN. On the left side of the force minimum, a repulsive feature with a magnitude of $+22$ pN emerges. At further distance reduction to $z = 150$ pm, shown in Fig. 2(c), the force image for the single atom tip becomes quite complex. A new repulsive feature emerges at the center, and the repulsive feature on the left-hand side appears as a crescent. The complex shape of single metal adatoms adsorbed on Cu(111) has recently been explained by Huber *et al.*, who acquired data of a single Si-, Cu-, and Fe adatoms on Cu(111) with a CO tip [13] and found that for the metal adatoms, strong hybridization between CO and the metal adatoms can occur. They report similar data to Fig. 2(c): A repulsive ring, surrounding an attractive inner ring and a repulsive feature in the center. The ring turns into a crescent when the tip is slightly tilted, as explained in the context of Fig. S6 in Ref. [13]. DFT calculations show that the repulsive ring with an attractive center is a complex phenomenon: Pauli repulsion between the CO tip and the Cu adatom prevails at the circumference, while for a CO tip that is exactly above the Cu adatom, hybridization occurs that leads initially to attraction, followed by Pauli repulsion for even smaller distances (see Fig. S3 in [13]).
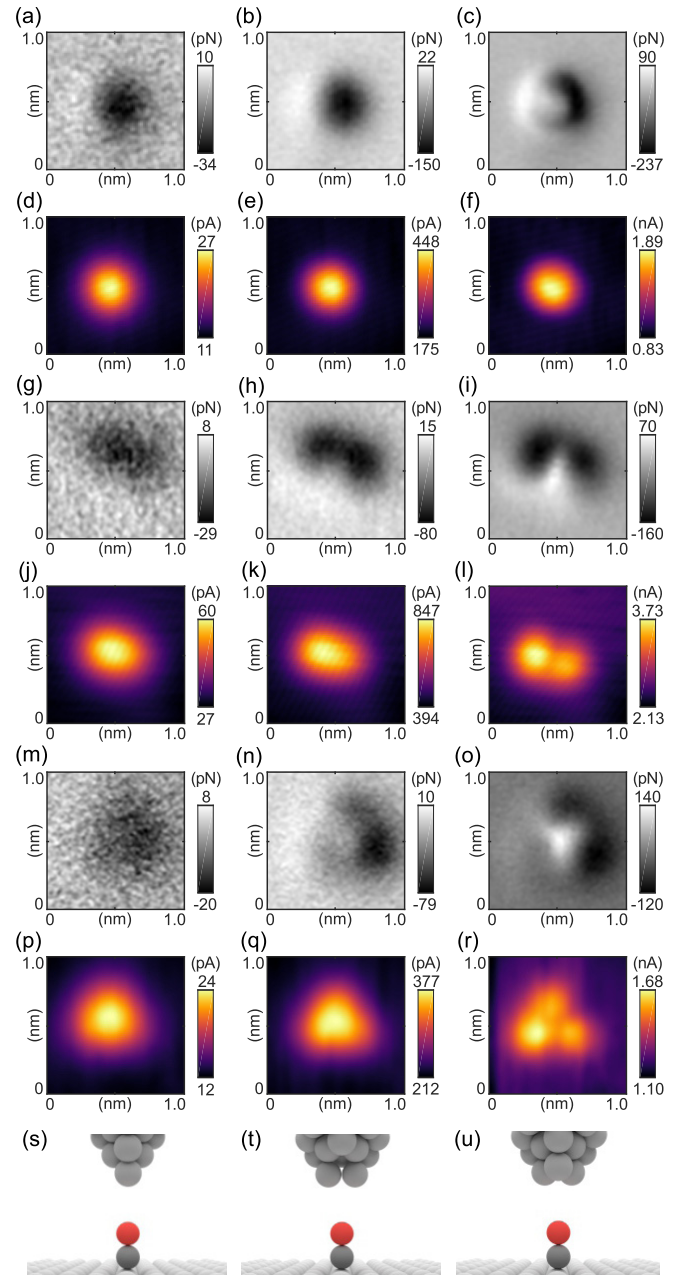

FIG. 2. (a)–(f): COFI of a single-atom tip at three different heights on Pt(111). F_z at (a) $z = 340$ pm, (b) $z = 220$ pm, (c) $z = 150$ pm. I at (d) $z = 340$ pm, (e) $z = 220$ pm, (f) $z = 150$ pm with bias voltage 1 mV. COFI of (g)–(l) a two-atom tip and (m)–(t) a three-atom tip: F_z at (g) $z = 340$ pm, (h) $z = 220$ pm, (i) $z = 150$ pm. I at (j) $z = 340$ pm, (k) $z = 220$ pm, (l) $z = 150$ pm with bias voltage 2 mV. F_z at (m) $z = 340$ pm, (n) $z = 220$ pm, (o) $z = 150$ pm. I at (p) $z = 340$ pm, (q) $z = 220$ pm, (r) $z = 150$ pm with bias voltage 2 mV. The bottom row is a schematic view of the CO on the surface and the single (s)-, two (t)- and three (u)-atom tips.

The STM images for the single-atom tip shown in Figs. 2(d), 2(e), and 2(f) are much easier to interpret. For all three heights a single feature of higher conductance can be seen, with almost identical lateral sizes. A discussion of the line profiles far and close to the CO will be done later.
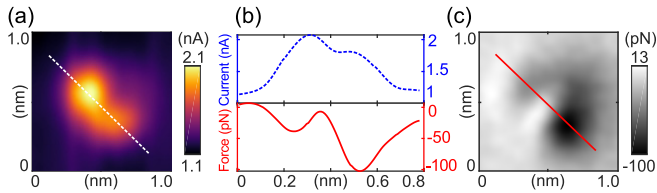
FIG. 3. A second two-atom tip dataset (a) STM image with a bias voltage of 4 mV. (b) Line profiles of the conductance and vertical force. (c) Corresponding vertical force image. The global maximum of the conductance line profile does not lie on top of the global maximum of the vertical force line profile.

FIG. 4. Comparison of frequency shift Δf (top row) and constant height STM current (bottom row) of two different one-atom tips at a bias voltage of 1 mV (left column) and 2 mV bias (right column).

Figures 2(g)–2(r) shows I and F_z images of tips ending in two and three atoms. Figures 2(s), 2(t), and 2(u) show schematic views of single-, two-, and three-atom tips. At a height of $z = 340$ pm, the two-atom tip appears as a single elongated attractive feature, shown in Fig. 2(g). At $z = 220$ pm, in Fig. 2(h), two distinct attractive features can be observed. Finally, at the closest approach, these two features are separated by a repulsive force ridge of 70 pN, shown in Fig. 2(i). As discussed previously, these two features indicate a two-atom tip [5,7,11]. The STM images of the two-atom tip can be seen in Figs. 2(j)–2(l). Here we can clearly make out two features at $z = 150$ pm.

Figures 2(m)–2(o) show F_z images of a three-atom tip. The vertical forces show a similar progression upon approach: At $z = 340$ pm [Fig. 2(m)], a single attractive feature is observed and at $z = 220$ pm [Fig. 2(n)], three distinct features start to emerge, which are more distinct at $z = 150$ pm [Fig. 2(o)].

Figures 2(p)–2(r) display the tunneling current image of the three-atom tip. At the closest distance in Fig. 2(r), three distinct features can be identified. The STM images in Figs. 2(l) and 2(r) are markedly different from data of CO molecules adsorbed on Cu(111) reported in Ref. [5]. On Cu(111), at low bias, STM images of CO molecules with a metal tip do not reveal individual atoms of the tip apex. The STM data must first be processed (e.g., by subtracting a Gaussian fit to the large depression as done in Fig. 2 of Ref. [5]) before atomic features can be seen. On Pt(111), the number and orientation of the atoms at the tip apex can be identified in both the FM-AFM and STM channels when scanning a metal tip over a single CO molecule.

Comparing the I and F_z data at closest approach for the two-atom tip [Figs. 2(i) and (l)] and three-atom tip [Figs. 2(o) and 2(r)], it can be seen that the atomic features with a greater attractive force do not necessarily correspond to one with higher conductance. The two attractive features in Fig. 2(i), each corresponding to one of the two atoms at the tip apex, have slightly different minima, with the one on the left having greater attraction. Similarly, the STM image at the same height [Fig. 2(l)] shows that the atom on the left has higher conductance. This pattern is not observed for the three-atom tip, where the lower-left atom has the least attraction, as can be seen in Fig. 2(o), and yet the highest conductance, shown in Fig. 2(r). Indeed, we have further datasets of multiple-atom tips, which do not show this trend. A second two-atom tip apex is shown in Fig. 3.
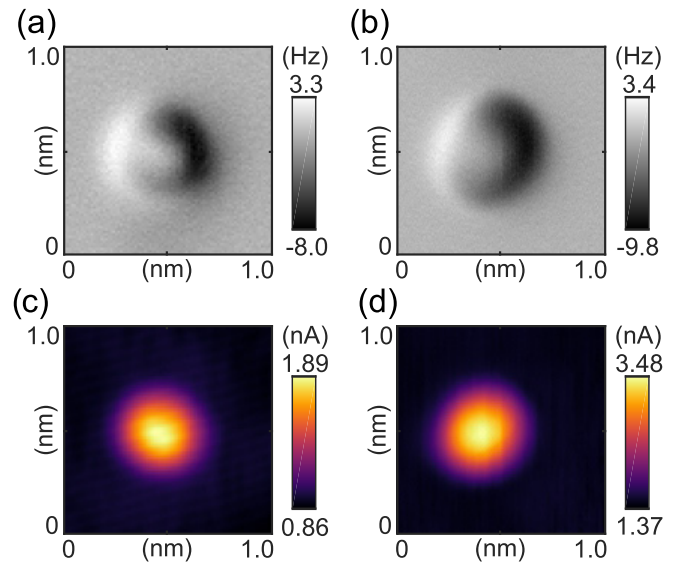
A line profile through the current and force is plotted in Fig. 3(b). There are two local minima in the force curve: Over the global minimum, the current is not maximal. The current reaches its global maximum over the second local minimum. We conclude that the atomic features do show a local maximum in I and local minimum in F_z, but that the intensity is a function of the tip shape and the higher-lying atomic layers, which we do not have access to.

In order to check for possible cross talk between current and force, we compared two data sets at the same height in Fig. 4 where the voltage and thus the current is doubled on the right column to 2 mV and about 3.5 nA with respect to the left column from 1 mV and about 1.9 nA, respectively, showing similar COFI images in both the FM-AFM channels (top row) and STM channel.

We will focus on the major difference between our STM data and previously published data of a CO adsorbed on Cu(111): The atomic resolution visible in the raw I images. Why is each atom clearly resolved when scanning over a single CO molecule on the Pt(111) surface, while this is not possible on Cu(111)? Possible reasons include the higher lateral stiffness of CO on Pt(111) or a different orbital electron tunneling contribution of the CO.

IV. INFLUENCE OF CO BENDING

It is well known that the flexibility of the CO molecule can affect FM-AFM images [2,28]. Persson previously presented the idea of considering the frustrated translational mode as the CO moving like a torsional spring [29]. Modelling the CO as a torsional spring has been an important component in understanding FM-AFM data with a functionalized tip [5,30–32]. The frustrated translational mode of CO is 5.94 meV [33,34] on Pt(111) compared to 4.2 meV [35] on Cu(111). This results in an effective lateral stiffness of a single CO
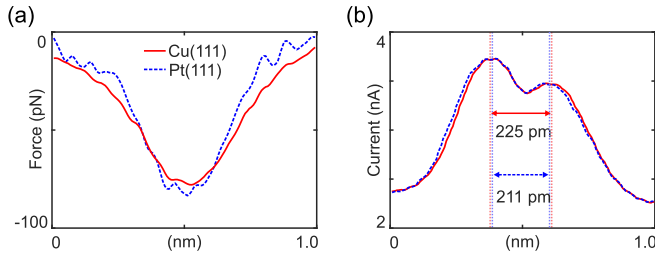
FIG. 5. (a) Force line profiles of single atom tips at heights with equal force minimum. (b) Line profiles of the current before (dashed blue curve) and after (red curve) correction of lateral distortion

molecule of 3.6 N/m on Pt(111) versus 1.7 N/m on Cu(111) as it can be shown by the following calculation.

CO adsorbed on Pt(111) or Cu(111) can be described by a torsional spring constant D and bending angle ϕ and the following differential equation as referenced in Ref. [5] supplemental:

$$(m_C(r_{Cu} + r_C)^2 + m_O(r_{Cu} + 2r_C + r_O)^2)\ddot{\phi} = -D\phi, \quad (5)$$

where r_{Cu}, r_C, and r_O are the covalent bonding radii of Cu, C, and O (128, 77, and 66 pm) [5]. By using the energies of the frustrated translational modes ($E_{Pt} = 5.94$ meV and $E_{Cu} = 4.2$ meV [33–35]), $\omega = E/\hbar$, as well as the relation for the lateral stiffness $k_{CO} = \frac{D}{(l_{CO})^2}$ [31], where l_{CO} is the distance between the center of the surface atom and the oxygen atom of the CO, the lateral stiffness k_{CO} can then be calculated by

$$k_{CO} = \frac{\omega(m_C(r_{Cu} + r_C)^2 + m_O l_{CO}^2)}{l_{CO}^2} \quad (6)$$

which results in values of 3.6 N/m on Pt(111) and 1.7 N/m on Cu(111).

One method to investigate the effect of CO bending on the FM-AFM data is to compare line scans of force of a single atom tip between a CO adsorbed on Cu(111) and on Pt(111), shown in Fig. 5(a). As expected, given the larger stiffness of CO on Pt(111), the width of the line profile is smaller than for the force profile on Cu(111).

Influence of CO bending on the STM image

To characterize the effect of bending of the CO molecule on the STM data, we extracted the lateral forces from the FM-AFM data with a method utilized in Ref. [23]. For the two-atom tip, the maximum lateral force is 79 pN, which corresponds to a lateral displacement (with the lateral spring constant of 3.6 N/m) of 22 pm. For the three-atom tip shown in Fig. 2(o), the maximum lateral force is 93 pN, which corresponds to a lateral displacement of 26 pm.

To quantitatively study the influence of CO bending during the acquisition of the STM images, we displaced every pixel in the STM image according to the lateral displacement vector, calculated by the lateral forces and the CO stiffness. Therefore, every pixel (x, y) in the STM image was displaced by a displacement vector $\vec{X}(x, y)$. Using the lateral forces $F_x(x, y)$, $F_y(x, y)$, the stiffness k_{CO}, and Hook's law, the displacement
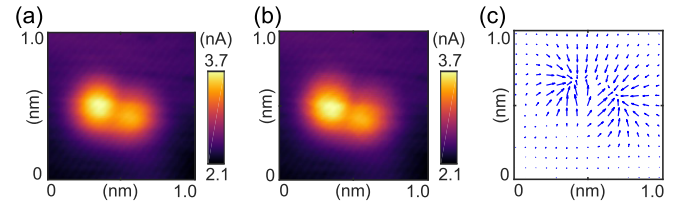

FIG. 6. (a) The raw two-atom STM image, (b) the corrected STM image, and (c) the vector field of the lateral forces.

vector $\vec{X}(x, y)$ can be calculated by

$$\vec{X}(x, y) = \frac{1}{k_{CO}}\begin{pmatrix} F_x(x, y) \\ F_y(x, y) \end{pmatrix} = \begin{pmatrix} q_1(x, y) \\ q_2(x, y) \end{pmatrix}. \quad (7)$$

F_x, F_y were calculated by taking the derivatives $-\partial U/\partial x, y$ of the deconvoluted potential energy $U(x, y)$ at $z = 150$ pm. $k_{CO} = 3.6$ N/m as derived above for CO on Pt(111). For, e.g., a two-atom tip each pixel at (x, y) of the STM image [Fig. 6(a)] was displaced by (q_1, q_2) and a new image was generated as depicted in Fig. 6(b). The differences are marginal and the STM image became more fuzzy. However the overall shape remains unchanged. By plotting the lateral forces F_x and F_y as a vector field, the magnitude and directions of the lateral forces can be seen [Fig. 6(c)]. The highest lateral forces do not lie above the current maxima.

Figure 5(b) displays a line scan of the STM data of the two-atom tip of both the raw data and the data corrected for the lateral displacement. The distance between the maxima is reduced from 225 pm to 211 pm, but the overall change to the profile is minimal.

A second demonstration that CO bending has a minimal effect on the STM signal is to compare the normalized current profile of a single atom tip far from the surface, where the bending is negligible, to the current profile close to the surface. The similarity of the two current profiles (shown in Fig. 7) shows that CO bending does not affect the STM image significantly.

Is it, however, possible that the softer CO on Cu(111) "smoothes out" the STM image of the two-atom or three-atom tip, thus preventing atomic resolution in the raw STM image?
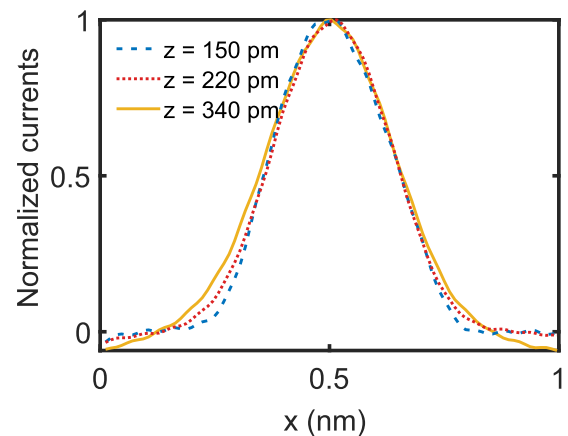

FIG. 7. Normalized line profiles of the STM images of a single-atom tip from Figs. 2(d)–2(f).

The short answer is no: We analyzed the raw data of two- and three-atom tips from Ref. [5] and found maximum lateral forces of 41 pN for the two-atom tip and 52 pN for the three-atom tip. With a lateral stiffness of CO on Cu(111) of 1.7 N/m, these lateral forces correspond to a lateral displacement of 24 and 31 pm, respectively, which are quite similar to the case of CO on Pt(111). Hence, they do not significantly alter the STM channel. This can also be seen in Ref. [5], Fig. 1 in which constant-height STM images are presented at various tip-sample distances. At further distances, the lateral forces are negligible, and yet the STM images do not drastically change. Therefore the resolution in the STM images on Pt(111) is not a result of a stiffer CO but rather is due to more localized electron tunneling.

V. THROUGH MOLECULE CURRENT

In order to demonstrate the through molecule current contribution, we can model the STM images of a two- and three-atom tip, if we assume that the tunneling through each atom is dominated by s waves. To do this, we modelled the tunneling current by a sum of s states [36]:

$$I(x, y, z) \propto \sum_i \frac{1}{\kappa r_i} e^{-\kappa r_i}, \tag{8}$$

where i represents each atom at the tip, and κ is the tunneling decay rate over the CO. The length of the vector from the surface to the tip atoms is given by $r_i = \sqrt{(x - x_i)^2 + (y - y_i)^2 + (z - z_i)^2}$, where x_i and y_i indicate the positions of the individual atoms evaluated from the STM images in Figs. 2(l) and 2(r). The height z_1 was set to 0 pm and images were evaluated at $z = 150$, 220, and 340 pm describing the height of the metal tip above the CO molecule. This is a larger tip-sample distance than determined by the quantum point contact method but yielded better agreement with the data. The decay rate κ was determined by fitting $I(z) \propto \exp(-2\kappa z)$ at the position of the current maxima for each tip in the closest STM image. For the two- and three-atom tip this yielded values for κ of 1.15×10^{10} m^{-1} and 1.25×10^{10} m^{-1}, respectively.

The resulting modelled images for the two-atom tip are shown in Figs. 8(a)–8(c). Here the atomic resolution at the closest image can clearly be seen. The intensity difference between the atoms is included in this model, by setting the height of the second atom to $z_2 = z_1 + 12$ pm. At a larger distance, the two distinct features are no longer distinguishable as evident in Figs. 8(a) and 8(b).

We also modelled the STM images for the three-atom tip, shown in Figs. 8(d)–8(f). Here, the atomically resolved features at the closest image can be observed [Fig. 8(f)]. The intensity difference could again be reproduced by a 12 pm offset of the positions of z_2 and z_3 relative to z_1. For greater
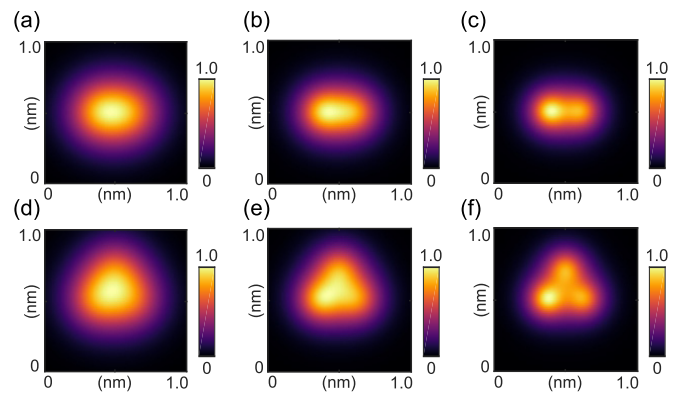

FIG. 8. Calculated STM images at three different heights 340, 220, and 150 pm (left to right). (a)–(c) Calculated STM images of a two-atom tip. (d)–(f) Calculated STM images of a three-atom tip. Values are normalized and relative to the maximum of the measured STM images.

tip-sample distances, the atomic features become less distinct as shown in Figs. 8(d) and 8(e). Although this model does not take the tunneling into the surface into account, it nonetheless reproduces the STM contrast shown in Figs. 2(l) and 2(r).

VI. CONCLUSION

In conclusion, we have shown that the atomic structure of the tip can be revealed by STM when probing CO/Pt(111) in contrast to CO/Cu(111), where AFM is needed to clearly resolve the tip apex. This feature rests on the highly localized conductance through the adsorbed molecule that in the case of CO/Pt(111), and the increased stiffness of the CO on Pt(111) is not the origin of the higher STM resolution. On Cu(111), an adsorbed CO apparently repels the surface states, which leads to a wide trough in the STM image. The higher density of states of the surface states at Fermi level on Cu(111) compared to the bulk states (ratio of $D_{2D}/D_{3D} = 1.19$) illustrate the dominating contribution of the surface state to the STM image. By simulating STM images on Pt(111), we were able to show that the images of two-atom and three-atom tip apexes could be reproduced by considering s waves at the position of each tip atom. In this system, the number and orientation of atoms at the apex of a metal tip can be quantified in raw STM images, allowing straightforward characterization of the tip apex in SPM experiments.

[1] L. Bartels, G. Meyer, and K. H. Rieder, Appl. Phys. Lett. **71**, 213 (1997).

[2] L. Gross, F. Mohn, N. Moll, P. Liljeroth, and G. Meyer, Science **325**, 1110 (2009).

[3] C. L. Chiang, C. Xu, Z. Han, and W. Ho, Science **344**, 885 (2014).

[4] B. De La Torre, M. Švec, G. Foti, O. Krejčí, P. Hapala, A. Garcia-Lekue, T. Frederiksen, R. Zbořil, A. Arnau, H. Vázquez, and P. Jelínek, Phys. Rev. Lett. **119**, 166001 (2017).

[5] J. Welker and F. J. Giessibl, Science **336**, 444 (2012).

[6] J. Welker, A. J. Weymouth, and F. J. Giessibl, ACS Nano **7**, 7377 (2013).

[7] M. Emmrich, F. Huber, F. Pielmeier, J. Welker, T. Hofmann, M. Schneiderbauer, D. Meuer, S. Polesya, S. Mankovsky, D. Ködderitzsch, H. Ebert, and F. J. Giessibl, Science **348**, 308 (2015).

[8] T. Hofmann, F. Pielmeier, and F. J. Giessibl, Phys. Rev. Lett. **112**, 066101 (2014).

[9] N. Okabayashi, A. Gustafsson, A. Peronio, M. Paulsson, T. Arai, and F. J. Giessibl, Phys. Rev. B **93**, 165415 (2016).

[10] A. Liebig, A. Peronio, D. Meuer, A. J. Weymouth, and F. J. Giessibl, New J. Phys. **22**, 063040 (2020).

[11] D. Z. Gao, J. Grenz, M. B. Watkins, F. F. Canova, A. Schwarz, R. Wiesendanger, and A. L. Shluger, ACS Nano **8**, 5339 (2014).

[12] A. Schwarz, A. Köhler, J. Grenz, and R. Wiesendanger, Appl. Phys. Lett. **105**, 011606 (2014).

[13] F. Huber, J. Berwanger, S. Polesya, S. Mankovsky, H. Ebert, and F. J. Giessibl, Science **366**, 235 (2019).

[14] A. Zangwill, *Physics at Surfaces* (Cambridge University Press, Cambridge, 1988).

[15] J. Wiebe, F. Meier, K. Hashimoto, G. Bihlmayer, S. Blügel, P. Ferriani, S. Heinze, and R. Wiesendanger, Phys. Rev. B **72**, 193406 (2005).

[16] S. Hunklinger, *Festkörperphysik* (Oldenbourg Wissenschaftsverlag GmbH, München, 2014).

[17] A. Jedidi, S. Rasul, D. Masih, L. Cavallo, and K. Takanabe, J. Mater. Chem. A **3**, 19085 (2015).

[18] S. D. Kevan, Phys. Rev. B **34**, 6713 (1986).

[19] S. O. Kasap, *Principles of Electronic Materials and Devices* (McGraw-Hill, New York, 2002).

[20] P. O. Gartland, S. Berge, and B. J. Slagsvold, Phys. Rev. Lett. **28**, 738 (1972).

[21] M. F. Crommie, C. P. Lutz, and D. M. Eigler, Nature (London) **363**, 524 (1993).

[22] R. K. Tiwari, D. M. Otálvaro, C. Joachim, and M. Saeys, Surf. Sci. **603**, 3286 (2009).

[23] M. Ternes, C. P. Lutz, C. F. Hirjibehedin, F. J. Giessibl, and A. J. Heinrich, Science **319**, 1066 (2008).

[24] M. L. Bocquet and P. Sautet, Surf. Sci. **360**, 128 (1996).

[25] F. J. Giessibl, Appl. Phys. Lett. **73**, 3956 (1998).

[26] J. E. Sader and S. P. Jarvis, Appl. Phys. Lett. **84**, 1801 (2004).

[27] S. Morita, F. J. Giessibl, and R. Wiesendanger, *Noncontact Atomic Force Microscopy* (Springer, Berlin, 2009).

[28] P. Hapala, G. Kichin, C. Wagner, F. S. Tautz, R. Temirov, and P. Jelínek, Phys. Rev. B **90**, 085421 (2014).

[29] B. N. J. Persson, Chem. Phys. Lett. **149**, 278 (1988).

[30] L. Gross, F. Mohn, N. Moll, B. Schuler, A. Criado, E. Guitián, D. Peña, A. Gourdon, and G. Meyer, Science **337**, 1326 (2012).

[31] A. J. Weymouth, T. Hofmann, and F. J. Giessibl, Science **343**, 1120 (2014).

[32] M. P. Boneschanscher, S. K. Hämäläinen, P. Liljeroth, and I. Swart, ACS Nano **8**, 3006 (2014).

[33] A. M. Lahee, J. P. Toennies, and C. Wöll, Surf. Sci. **177**, 371 (1986).

[34] B. H. Choi, A. P. Graham, K. T. Tang, and J. P. Toennies, J. Chem. Phys. **112**, 10538 (2000).

[35] J. Braun, A. P. Graham, F. Hofmann, W. Silvestri, J. P. Toennies, and G. Witte, J. Chem. Phys. **105**, 3258 (1996).

[36] C. J. Chen, *Introduction to Scanning Tunneling Microscopy* (Oxford University Press, New York, 1993).